THE JOURNAL OF PHYSICAL CHEMISTRY C
Article
pubs.acs.org/JPCC

Dopant Diffusion in Sequentially Doped Poly(3-hexylthiophene) Studied by Infrared and Photoelectron Spectroscopy

Patrick Reiser,*[†,‡] Lars Müller,[‡,§,∥] Vipilan Sivanesan,[‡,§] Robert Lovrincic,[‡,∥] Stephen Barlow,[⊥] Seth R. Marder,[⊥] Annemarie Pucci,[‡,§,#] Wolfram Jaegermann,[†,‡] Eric Mankel,[†,‡] and Sebastian Beck*[‡,§]

[†]Materials Science Department, Surface Science Division, TU Darmstadt, Otto-Berndt-Straße 3, 64287 Darmstadt, Germany
[‡]InnovationLab, Speyerer Straße 4, 69115 Heidelberg, Germany
[§]Kirchhoff Institute for Physics, Heidelberg University, Im Neuenheimer Feld 227, 69120 Heidelberg, Germany
[∥]Institute for High-Frequency Technology, TU Braunschweig, Schleinitzstr. 22, 38106 Braunschweig, Germany
[⊥]Center for Organic Photonics and Electronics and School of Chemistry and Biochemistry, Georgia Institute of Technology, Atlanta, Georgia 30332-0400, United States
[#]Centre for Advanced Materials, Heidelberg University, Im Neuenheimer Feld 225, 69120 Heidelberg, Germany

Supporting Information

ABSTRACT: The diffusivity of dopants in semiconducting polymers is of high interest as it enables methods of sequential doping but also affects device stability. In this study, we investigate the diffusion of a bulky sequentially deposited p-dopant in poly(3-hexylthiophene) (P3HT) thin films using nondestructive *in situ* infrared (IR) spectroscopy and photoelectron spectroscopy (PES). We probe dopant diffusion into the polymer film at varying coverage by differentially evaluating electron transfer in the bulk and at the surface. Thereby it is possible to determine dopant coverages at which both electron transfer and incorporation of dopants are saturated. By use of PES, neutral and charged dopants can be distinguished, revealing that charged dopants are less mobile in the diffusion process than neutral molecules. We further compare the diffusivity in semicrystalline and fully amorphous P3HT. We find that at high coverage semicrystalline P3HT seems to yield a higher capacity for dopants than fully amorphous P3HT. A temperature-dependent measurement of sequential doping shows directly that the incorporation of dopants is thermally activated and requires temperatures close to room temperature.

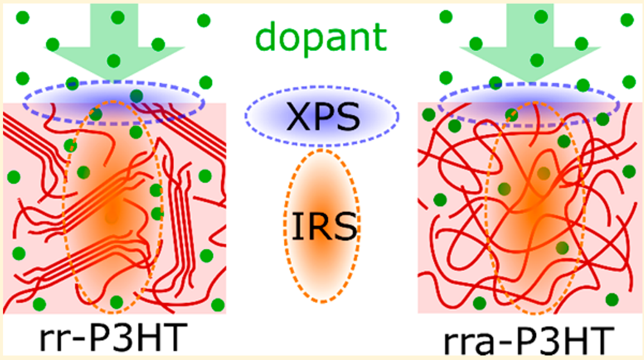

■ INTRODUCTION

Doping of organic semiconductors can significantly increase the free charge-carrier concentration, which usually results in a rise in conductivity.[1] This allows for specifically designing electronic properties[1,2] of charge-transport layers[3,4] and for reducing contact resistances by creating ohmic junctions[5,6] to various metals or metal-like oxides.[7,8] By improving the electronic properties of conjugated organic polymers, they also become promising candidates for use in low-cost thermoelectric applications due to their low thermal conductivity.[9−12]

However, the diffusivity of dopants is expected to negatively affect the lifetime and long-term stability of many types of organic electronic devices.[13] It is known that dopants can cause exciton quenching in photoactive layers[14−17] and at donor−acceptor interfaces, which reduces the efficiency of organic light-emitting diodes, organic solar cells, or organic photodiodes. In early studies, halogens[18] and alkali metals[19] were used to successfully dope polymers. However, due to their small size and high volatility, in the case of halogens, they were found to be disadvantageous for creating stable p−n structures.[20] Small molecular dopants are larger and seemingly less mobile and can achieve doping efficiencies around 40% for low concentrations.[21] Typical molecules for p-doping like 2,3,5,6-tetrafluoro-7,7,8,8-tetracyanoquinodimethane (F_4TCNQ) and molybdenum tris(1,2-bis(trifluoromethyl)-ethane-1,2-dithiolene) ($Mo(tfd)_3$) possess a high electron affinity and enable an integer or partial electron transfer from the host molecule.[22] In addition to the exact charge-transfer mechanism,[22−24] drift and diffusion of molecular dopants and their reactions at interfaces gained more attention recently.[25−30] For conjugated host molecules stable doped layers

Received: March 19, 2018
Revised: June 7, 2018
Published: June 8, 2018

DOI: 10.1021/acs.jpcc.8b02657

have been achieved with F_4TCNQ and $Mo(tfd)_3$ in *N,N*′-di(1-naphthyl)-*N,N*′-diphenyl-(1,1′-biphenyl)-4,4′-diamine (α-NPD).[31,32] In more crystalline materials like zinc phthalocyanine (ZnPc) and 4,4′-bis(*N*-carbazolyl)-1,1′-biphenyl (CBP), F_4TCNQ was still found to diffuse toward a metal electrode modifying its surface potential.[27,28] In polymers, however, a much higher diffusivity of dopants is usually observed than in small molecular host materials, which makes stable doping more difficult. On the other hand, the high mobility of dopants in polymers can be beneficially used for sequential doping.[11,33,34] Here, it is possible to evaporate or solution-process mobile dopants on top of already produced thin films. This enables at the same time doped and, at least in some cases, highly ordered polymer films with coherent charge transport.[26,35] In order to prevent unwanted diffusion after sequential doping, certain strategies have been proposed.[29,36,37] To suppress an intermixing of adjacent layers, an additional dopant-confining interlayer can be introduced by soft-contact transfer lamination.[36] The interlayer is formed from a blend of a polymer and a fullerene acceptor, which presumably fills the diffusion path of the dopant.[36]

In general, it is perceived that the diffusion depends on both size and shape of the dopant as well as on the host material. In this context, observations of thermally activated diffusion of dopants in conjugated molecular hosts generally show that larger dopants have better morphological stability.[25] Regarding blends for organic solar-cell applications, the diffusion of a fullerene derivative in the hole-transporting polymer poly(3-hexylthiophene) (P3HT) was quantitatively analyzed, and diffusion constants *D* of $\sim10^{-11}$ and $\sim10^{-14}$ $cm^2\ s^{-1}$ at around 140 °C were obtained.[38−40] As another example, the diffusion constants of ions in polymers from electrolyte dielectrics used in organic thin-film transistors were evaluated to be 10^{-12}–10^{-14} $cm^2\ s^{-1}$ at room temperature.[41,42] Very recently, also the diffusion constant of the dopant F_4TCNQ and a derivative in which one of the cyano moieties is replaced by an alkyl ester group was measured in P3HT using confocal fluorescence microscopy.[43] It was found that charged F_4TCNQ ($D = \sim10^{-13}$ $cm^2\ s^{-1}$) is less mobile than neutral F_4TCNQ ($D = \sim10^{-11}$ $cm^2\ s^{-1}$) and that its monoester-substituted derivative is more than 1 order of magnitude less mobile than the parent F_4TCNQ.[43] However, fewer studies have focused on how the host morphology and doping concentration may affect the diffusivity of dopants. Diffusion of solvents and other liquid small molecules in rubbery or glassy polymers has been widely studied in the literature.[44,45] The penetration of solvents into polymers is frequently described by models based on free-volume[46,47] and partial immobilization concepts.[48−50] The temperature dependence of the diffusion in such systems can be best described by Arrhenius law and involves an activation energy for transport.[44] Consequently, similar phenomena could be expected for solid-state dopants, taking into account neutral and charged penetrants.

In this study, the diffusion of the soluble $Mo(tfd)_3$ derivative molybdenum tris(1-(methoxycarbonyl)-2-(trifluoromethyl)-ethane-1,2-dithiolene) ($Mo(tfd\text{-}CO_2Me)_3$)[51,52] is investigated following its evaporation onto P3HT thin films with varying crystallinity in a sequential doping scheme. We use in situ IR spectroscopy during the sequential dopant deposition and subsequent photoemission spectroscopy to monitor the whole diffusion process since both techniques are capable of detecting bulk and interface doping.[53−55] As $Mo(tfd\text{-}CO_2Me)_3$ is larger than, for example, F_4TCNQ, the dopant is expected to be unable to enter the π−π stacking of P3HT crystallites below the glass-transition temperature, which may affect the diffusion behavior when comparing different morphologies. By applying *in situ* IR spectroscopy during the preparation process, an instantaneous doping, independent of the polymer crystallinity, was observed for low coverage. By cooling the substrate and the polymer film prior to dopant evaporation and in situ monitoring during the warm-up, the thermal activation of the diffusion process was identified. Further X-ray photoelectron spectroscopy (XPS) measurements show a difference in the diffusion properties for high coverage of $Mo(tfd\text{-}CO_2Me)_3$ in regioregular P3HT (rr-P3HT) compared to regiorandom P3HT (rra-P3HT) thin films. The changes observed in the molar doping ratios at the surface of the polymer film can be described by a simple analytical diffusion model and suggest a lower diffusivity in rra-P3HT for high concentrations. A possible explanation could involve a higher free volume in grain boundaries or connecting amorphous regions of the semicrystalline P3HT.

■ EXPERIMENT

Materials. For all films discussed below, rr-P3HT from Merck (>93% regularity, M_W = 24 kg mol^{-1}) and rra-P3HT from Rieke Metals (M_W = 57 kg mol^{-1}) were used without further treatment. The dopant $Mo(tfd\text{-}CO_2Me)_3$ was synthesized and purified as previously described.[51] The chemical structures of P3HT and $Mo(tfd\text{-}CO_2Me)_3$ can be found in Figure 1. The polymer materials were dissolved in analytical grade chlorobenzene and were stirred on a hot plate at 50 °C

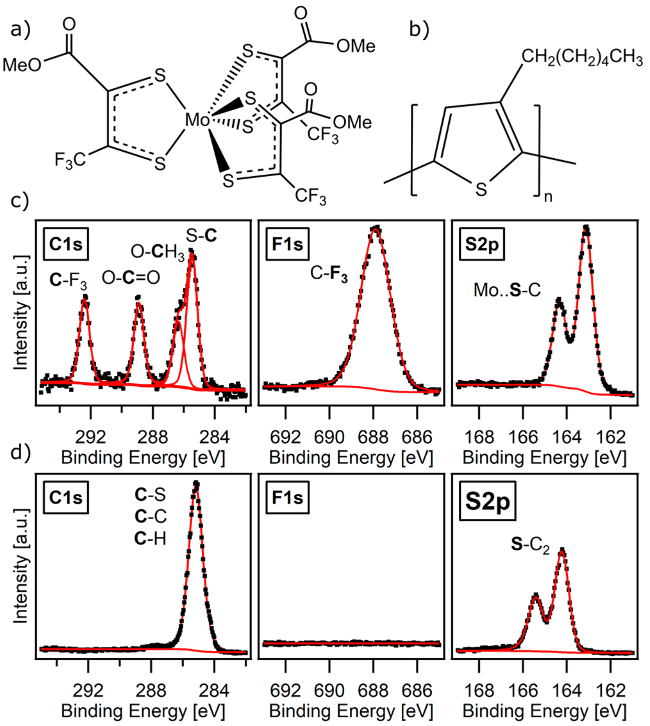

Figure 1. Figure shows the structural formula of $Mo(tfd\text{-}CO_2Me)_3$ (a) and P3HT (b) with corresponding XPS core-level spectra of a pure $Mo(tfd\text{-}CO_2Me)_3$ layer in (c) and a pure P3HT layer in (d). The peak components of the C 1s emission of $Mo(tfd\text{-}CO_2Me)_3$ can be clearly assigned to the distinct carbon species in binding energy and intensity ratio. The C 1s inset in (c) is expanded in intensity compared to the C 1s spectrum in (d).

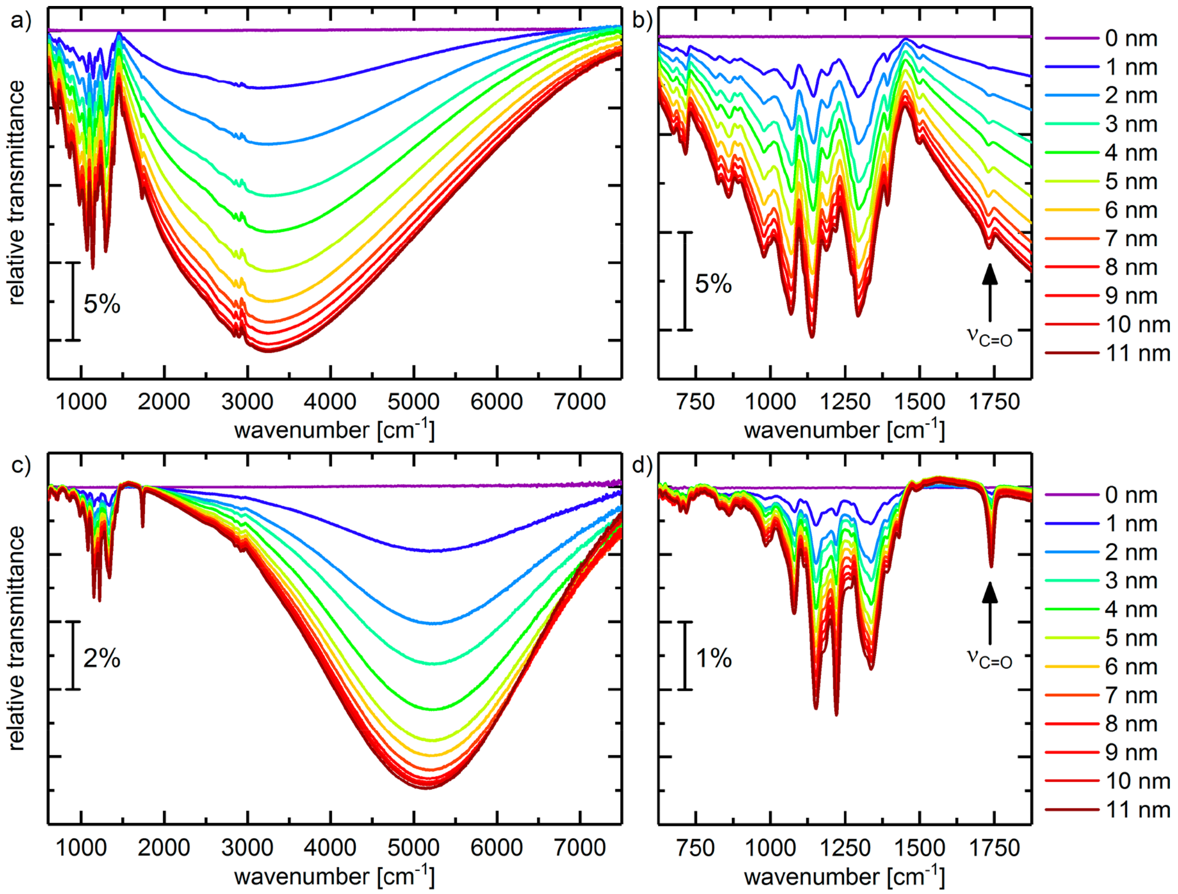

Figure 2. Relative transmission spectra of a sequentially doped rr-P3HT layer for varying dopant coverage from 0 to 11 nm in the whole MIR range (a) and in the fingerprint range (b). Relative transmission spectra of a sequentially doped rra-P3HT layer for varying dopant coverage from 0 to 11 nm in the whole MIR range (c) and in the fingerprint range (d). The characteristic C═O stretching vibration of Mo(tfd-CO_2Me)$_3$ is marked on the right. Note the different ordinate scales of (a–d).

for at least 20 h. The concentrations of rra-P3HT and rr-P3HT solutions were set to 11 and 13.5 mg mL^{-1}, respectively. We used 1.5 × 1.5 cm^2 cut silicon wafers (intrinsic, $\sigma > 5000\ \Omega$ cm) with a native oxide layer as substrates. The silicon substrates were cleaned with acetone and isopropanol in an ultrasonic bath for 30 min.

Sample Fabrication. The P3HT solutions were directly spin-cast at 1200 rpm for 30 s in a nitrogen glovebox with both water content and oxygen concentration below ca. 10 ppm. Subsequently, the backside of the substrate was cleaned with chlorobenzene, and the sample was briefly exposed to ambient conditions in a clean room during transfer to the evaporation chamber. After evaporation, ultrahigh vacuum (UHV) conditions were maintained for XPS and IR studies. The initial film thickness was measured with ellipsometry and a DEKTAK profilometer to be $L_0 = 50 \pm 6$ nm. The dopant Mo(tfd-CO_2Me)$_3$ was evaporated at a pressure of 10^{-8} mbar and adsorbs on organic materials as well as on silicon at room temperature in UHV.

IR Spectroscopy. All samples for IR transmission measurements were prepared and measured in situ in an UHV chamber that is connected to a Fourier-transform IR spectrometer (Vertex 80v) from Bruker. The complete beam path was evacuated to 3 mbar to prevent absorption from ambient air (water and CO_2). A mercury–cadmium–telluride (MCT) detector and a resolution of 4 cm^{-1} were used for spectra acquisition, and 200 scans were averaged for each spectrum. The deposition rates for the dopant molecules were set between 0.1 and 1 nm min^{-1} and were monitored by a quartz crystal microbalance. The resulting nominal layer thickness L_d then provides a measure of the total amount of dopants deposited.

X-ray Photoemission Spectroscopy (XPS). For XPS measurements Mo(tfd-CO_2Me)$_3$ was evaporated at a rate of ca. 1 nm min^{-1} onto the pristine P3HT films, which were subsequently transferred to the XPS chamber. Core-level spectra were recorded over time employing a PHI 5000 Versa probe scanning photoelectron spectrometer equipped with a monochromated Al Kα X-ray source. The binding energy is referenced to the Fermi edge of a sputter-cleaned silver surface. The focused X-ray beam (200 μm diameter) was moved along the surface within one data series to avoid radiation damage. The combined background-subtracted core-level emission of carbon, sulfur, and fluorine, shown in Figure 1, can be used to determine the molar concentration at the surface.

Data Analysis. In order to calculate element ratios, the area of each core level peak I is weighted with atomic sensitivity factors $\tilde{I} = I/\mathrm{ASF}$, which are specific to the spectrometer and account for analyzer transmission, cross section, and average electron mean free path. Since both dopant and matrix contain sulfur and carbon, the molar ratio of dopants n_d to matrix monomers n_m is inferred from solving

$$\frac{\tilde{I}(\mathrm{F\ 1s})}{\tilde{I}(\mathrm{C\ 1s,\ S\ 2p})} = \frac{N_{\mathrm{d}}(\mathrm{F})n_{\mathrm{d}}}{N_{\mathrm{m}}(\mathrm{C,\ S})n_{\mathrm{m}} + N_{\mathrm{d}}(\mathrm{C,\ S})n_{\mathrm{d}}} \tag{1}$$

where N_d(C,F,S) and N_m(C,S) denote the number of atoms (C, F, S) in dopant and matrix monomers, respectively. Uncertainties in carbon and sulfur intensities lead to comparably large errors at high molar ratios of dopants. Therefore, a peak component fit of the C 1s emission is used instead of eq 1, attributing the carbon species to Mo(tfd-$CO_2Me)_3$ or P3HT (see Figure 1).

■ RESULTS

IR Analysis. The diffusion of dopant molecules into P3HT layers throughout the sequential doping process was monitored by *in situ* IR spectroscopy. For this purpose, IR spectra of P3HT layers on silicon substrates were measured in transmission geometry before and continuously during the thermal deposition of Mo(tfd-$CO_2Me)_3$. In Figure 2 relative transmission spectra of sequentially doped P3HT layers for varying dopant coverage from 0 to 11 nm are shown. The spectrum of the undoped P3HT was used as reference and is given in the Supporting Information (see Figure S1). Broad polaronic absorption bands around 3250 cm^{-1} for rr-P3HT and around 5000 cm^{-1} for rra-P3HT, as well as strong IR-active vibrational (IRAV) modes below 1500 cm^{-1}, which are typical doping-induced spectral changes, can be observed with increasing dopant coverage for both types of P3HT.[56] These spectral features are attributed to electron transfer from the P3HT to the dopant molecules, resulting in a positively charged polymer backbone, i.e., the formation of positive polarons. The blue-shift in the excitation energy of the polaron feature for rra-P3HT compared to rr-P3HT is caused by the stronger localization of the polaron due to the lower conjugation length along the polymer chain and the suppressed intermolecular $\pi-\pi$ stacking.[56] Most of the vibrational modes of Mo(tfd-$CO_2Me)_3$ are relatively weak compared to the strong IRAV modes of the polymer (see Supporting Information or Figure 3b for IR spectrum of Mo(tfd-$CO_2Me)_3$). Therefore, only the characteristic C═O stretching vibration at 1735 cm^{-1}, which is well-separated from the IRAV modes of P3HT, can be used as indicator of the presence of dopant molecules in the doped layer (see Figure 2b,d). The spectra reveal that the doping and, thus, also the diffusion of dopant molecules start simultaneously with the evaporation for both types of P3HT. The strongest spectral changes can be observed for low coverage followed by a continuous saturation for higher coverages. For very high coverages above 8 nm there are almost no additional doping-induced changes, but the vibrational modes of neutral dopant molecules can be detected (see Figures S2 and S3). This observation does not depend on the polymer crystallinity and implies that a further deposition of dopant molecules does not induce additional electron-transfer reactions. Because IR spectroscopy probes the whole layer stack and the spectral resolution of the experiments is limited to 4 cm^{-1}, we cannot distinguish between the formation of an adlayer of neutral Mo(tfd-$CO_2Me)_3$ on top of the P3HT layer and neutral dopant molecules that are diffusing into the P3HT layer.

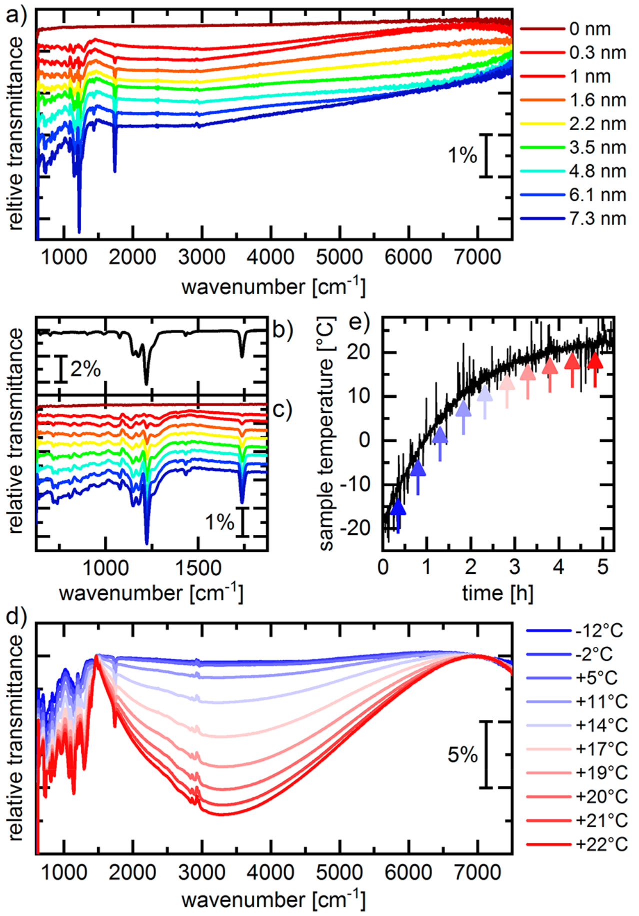

Figure 3. Relative transmission spectra of a sequentially doped rr-P3HT layer (cooled to −80 °C during Mo(tfd-$CO_2Me)_3$ deposition) for varying dopant coverage from 0 to 7.3 nm in the whole MIR range (a) and in the fingerprint range (c). For comparison, a relative transmission spectrum of a thermally deposited 19 nm thick Mo(tfd-$CO_2Me)_3$ layer is shown in (b). Baseline corrected relative transmission spectra of a cooled and sequentially doped rr-P3HT layer measured during warm-up to RT are given in (d). (e) Evolution of the sample temperature during the warm-up. The temperatures for the shown spectra in (d) are marked with arrows and are coded by colors given in the legend.

To ensure that the observed doping of P3HT at room temperature (RT) is not only a surface-doping effect and to demonstrate the thermally activated character of the proposed diffusion process, we performed temperature-dependent IR measurements. Prior to dopant evaporation the substrate (silicon + rr-P3HT) was cooled to −80 °C using liquid nitrogen, and IR spectra were measured in transmission geometry before and continuously during the deposition process as shown in Figure 3.

Because of the decreased substrate temperature, the ability for dopant diffusion into the P3HT should be strongly suppressed, and a layer of the pure dopant on top of the pure rr-P3HT layer can be expected. The spectrum for a nominal dopant coverage of 0.3 nm shows the characteristic spectral changes (IRAV modes + polaron), indicating electron transfer at the interface between P3HT and the dopant adlayer. For higher coverages the vibrational modes of the neutral dopant molecule clearly can be observed as deduced from the comparison of the spectra in the fingerprint range in Figure 3c and the spectrum of a layer consisting only of Mo(tfd-$CO_2Me)_3$ in Figure 3b. When the sample is warmed up, drastic spectral changes occur as shown in Figure 3d. With increasing sample temperature the polaron feature at around 3250 cm^{-1}, and the IRAV modes below 1500 cm^{-1}, significantly increase in intensity. Both features saturated when the sample reached

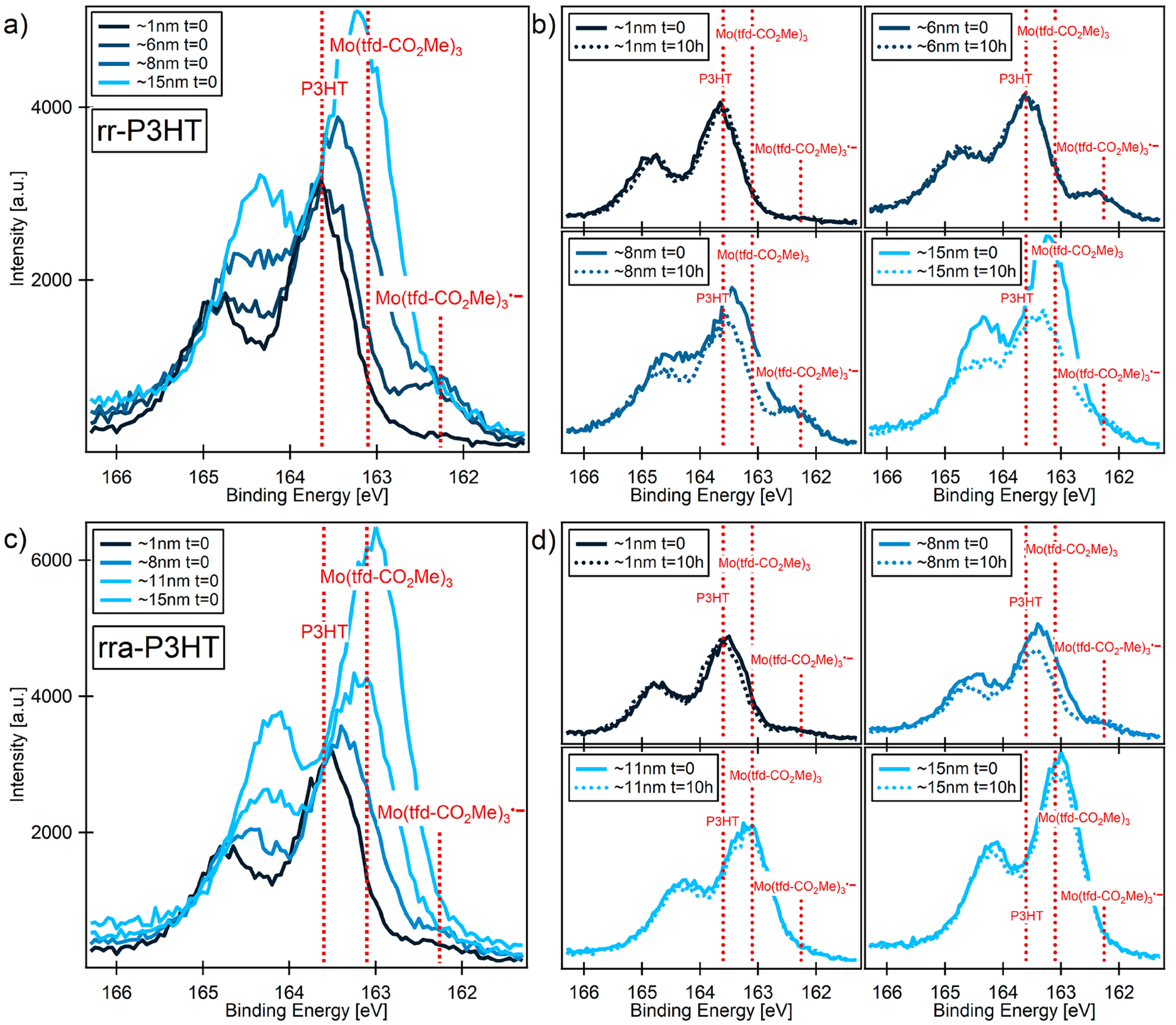

Figure 4. Sulfur 2p core-level spectra for rr-P3HT (a) and rra-P3HT (c) with varying dopant coverage directly after dopant evaporation. Time-dependent sulfur 2p core-level spectra for rr-P3HT (b) and rra-P3HT (d). The solid lines show the spectra recorded directly after evaporation, and the dashed lines show the spectra recorded 10 h later. The assignment of the S $2p_{3/2}$ emission line for different chemical components is marked in red in each plot. The shift of the core level line with deposited amounts of Mo(tfd-CO_2Me)$_3$ is also affected by a Fermi level shift in the sample with doping, especially compared to pure P3HT (not shown here).[59]

RT (after 3 h). This observation clearly reveals that a thermally activated diffusion process takes place. By evaluating the relative transmittance at IRAV mode and polaron peak positions with respect to the sample temperature, the onset temperature for the diffusion can be determined to occur in the range from 5 to 10 °C (see Figure S4). In addition to the increased thermal energy of the dopant molecules, the initiation of the diffusion process might also be related to a glass transition in the P3HT layer which was reported to take place in this temperature range.[57] Interestingly, from the comparison of IR spectral features of different sequentially doped rr-P3HT layers (from solution or evaporation at RT or at −80 °C and warming up afterward) it is evident that the total number of transferred electrons does not depend on the doping conditions details within the limits of accuracy (see Figure S5).

In conclusion, IR spectroscopy revealed doping-induced spectral changes indicating the diffusion of dopant molecules into neat layers of P3HT. At RT the instantaneous evolution of these features during the short evaporation procedure (20−30 min) implies a rather fast diffusion, at least of the small amount of dopant molecules that are relevant for the doping process, independent of the P3HT crystallinity. For higher coverages a further deposition of dopant molecules does not induce additional electron transfer, and presumably a dopant adlayer is formed. Thermal activation of the diffusion process was demonstrated by monitoring the deposition of Mo(tfd-CO_2Me)$_3$ onto a cooled rr-P3HT layer and the subsequent warming up of the bilayer to RT. But, since IR spectroscopy probes the whole layer stack, this method is not able to detect the diffusion profile of neutral and charged dopant molecules inside the P3HT layer. Because the migration of dopants is an important degradation mechanism in organic electronic devices,[13,16] in the following it will be inspected with XPS how chemical composition in a limited surface region changes with time for various initial dopant layer thicknesses.

XPS Analysis. Photoemission spectroscopy provides information complementary to that obtained from IR spectroscopy after deposition, as it is a surface-sensitive technique. Chemical states are detected only at the surface with an information depth of only a few nanometers, and neutral and charged dopants can be distinguished.

In Figure 4a,b the high-resolution spectra of the sulfur S 2p emission of sequentially doped rr-P3HT and rra-P3HT are plotted for varying nominal dopant coverage. The relative amount of sulfur in a Mo(tfd-$CO_2Me)_3$ molecule is higher than in a P3HT monomer, which leads to an overall increase in the S 2p intensity as the molar density of sulfur increases with increasing dopant concentration. Moreover, electron transfer from P3HT to the dopant molecule leads to an additional negative charge on the functional core of the metal complex, in particular on the C_2S_2 portions of dithiolene ligands.[32,58] Consequently, the core-level energy of the sulfur atoms of the complex is significantly affected, and the shoulder toward lower binding energy can be assigned to Mo(tfd-$CO_2Me)_3^{\bullet -}$, as marked in Figure 4. First, the amount of charged dopants at the surface increases with increasing coverage, meaning that most dopants detected at the surface are charged. This holds up to a coverage which corresponds to an equivalent nominal thickness of pure dopant of $L_d \approx 5$ nm, monitored by a microbalance. For higher coverages of rr-P3HT with Mo(tfd-$CO_2Me)_3$, additional charge transfer does not occur at the surface, which suggests an accumulation of neutral dopants. Moreover, the total amount of charged dopants seems to be lower in the case of rra-P3HT in comparison to rr-P3HT.

To study the further evolution of dopant concentration at the thin-film surface, XPS measurements were performed for various waiting times with the sample being at room temperature. For rr-P3HT these measurements reveal a clear continuous decrease of the uncharged surface fraction for coverages above 6 nm (see Figure S6). The decrease can be clearly seen in Figure 4b, where the S 2p core level spectra are plotted directly after the evaporation and 10 h later. This observation indicates that the dopants diffuse into the rr-P3HT layer. The corresponding measurements on rra-P3HT show that this effect is much less pronounced (see Figure 4d). But, it should be mentioned that the shoulder toward lower binding energies does not further decrease with waiting time for either type of P3HT regardless of the dopant coverage, which suggests that charged dopants do not leave the probed area although we do not expect an even dopant distribution in the film. This indicates that neutral dopants are more mobile than charged dopants, which are likely Coulombically bound to the host matrix.

To investigate the diffusion process of the neutral molecular species in more detail, a comprehensive analysis of the surface ratio of dopant molecules to P3HT monomers was conducted according to eq 1. In Figure 5, the surface fraction as obtained from XPS data analysis is plotted versus waiting time (on a log scale) for the various nominal dopant coverages (quantified by a corresponding dopant layer thickness, L_d). A dense adlayer of dopants could be expected if there were only dopant molecules detected within the inelastic electron mean free path of a few nanometers. But, the measured molar ratio of Mo(tfd-$CO_2Me)_3$ to P3HT monomers at the surface shows that there is in fact no dense adlayer of Mo(tfd-$CO_2Me)_3$ present at the surface (already at the first XPS measurement) up to a nominal dopant layer thickness of 18 nm for rr-P3HT and 14 nm for rra-P3HT. This observation agrees with IR results where the penetration of dopant molecules into the P3HT film was already seen during evaporation. A further decrease of the dopant surface concentration, derived from F 1s and C 1s emission spectra, can be observed in Figure 5 for rr-P3HT and less pronounced for rra-P3HT at certain coverages. The decreasing amount of dopants in the surface layer can be explained by either desorption or slow diffusion of the dopant molecules into the bulk. From a desorption measurement of a thin film of Mo(tfd-$CO_2Me)_3$ on Si we estimated a desorption rate $r \lesssim 0.05$ nm h^{-1} (see Figure S7). This estimate is further corroborated by IR measurements and suggests that the decrease in dopant concentration seen in the XPS data is primarily due to diffusion.

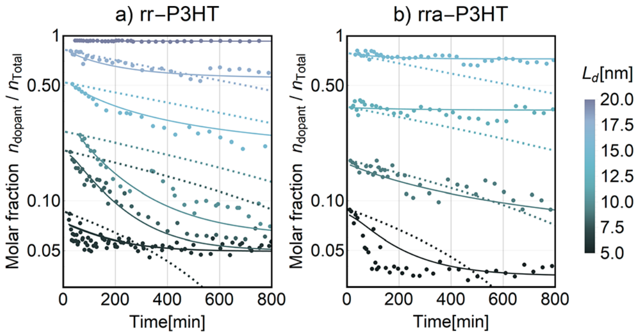

Figure 5. Surface molar fractions of Mo(tfd-$CO_2Me)_3$ to P3HT monomers for rr-P3HT (a) and rra-P3HT (b). The color legend on the right side indicates the approximate nominal layer thickness L_d of Mo(tfd-$CO_2Me)_3$. The solid lines represent the fit according to the model in eqs 2−4. Relative errors for molar ratios can be estimated to be as high as 15%. The dashed lines represent an estimate of desorption considering a top layer of dopants on pure P3HT with a desorption rate of $r = 0.05$ nm h^{-1} (for details see the Supporting Information).

Time-dependent changes of the surface concentration of a solution-doped P3HT film (with a similar average but homogeneous dopant distribution) were not observed in UHV (see Figure S8).

The decrease in molar surface fraction as it is depicted in Figure 5 is now compared to a one-dimensional model that is formulated in terms of concentration c and accounts for dopant absorption, bulk diffusion of dopants, charging of dopants, and a finite sorption capacity of the thin film. The model is applied to XPS data taken with the samples at room temperature, i.e., about 5−10 min after the deposition process that likely differs in temperature and kinetics. From the nominal dopant layer thicknesses L_d (calculated from the deposition rate and time) of the various samples we estimated the amount of dopants n_d from which molar fractions $n_d/(n_d + n_m)$ is calculated by using the respective molecular weight and an approximate density for Mo(tfd-$CO_2Me)_3$ and P3HT (for details see the Supporting Information). Molar fractions are locally proportional to molar concentrations c if a mean density and molar weight is introduced. Therefore, molar concentrations directly correspond to the experimentally derived molar fractions plotted in Figure 5. The total film thickness L for this simulation is approximated by $L = L_d + L_0$, where L_0 denotes the initial thickness of the pristine P3HT film. Within the model we distinguish between the concentration of charged dopants c_c, neutral mobile dopants c_n, and dopants adsorbed only at the surface c_a. The surface region at which c_a is defined is set to 3 nm, which roughly matches the information depth of XPS as well as the surface roughness of P3HT. In this region, dopants from the surface are expected to be absorbed and, in our model, transformed to neutral, mobile dopants. From Figure

4b,d we have deduced that changes in surface concentration are mainly governed by neutral dopants and that the amount of charged dopants remain constant with time. Consequently, we treat charged dopants as immobile and only neutral dopants to be diffusive. The bulk diffusion of neutral dopants is approximated by a Fickian diffusion with a diffusion constant D_c that is independent of concentration and the diffusion current is set to zero at the boundary of the thin film. For simplicity, absorption or uptake of dopants and charging of neutral dopants are modeled by linear isothermal sorption (in eqs 3 and 4) including a saturation capacity.[60] The total capacity of dopants in P3HT is denoted by S_{tot}, and the upper bound of the charged fraction is given by S_c. The coupled system of differential equations then reads as

$$\partial_t c_n(x, t) = D_c \partial_x^2 c_n(x, t) - \partial_t c_c(x, t) - \partial_t c_a(x, t) \tag{2}$$

$$\partial_t c_c(x, t) = k_c c_n(x, t)\left(1 - \frac{c_c(x, t)}{S_c}\right) \tag{3}$$

$$\partial_t c_a(x, t) = -k_a c_a(x, t)\left(1 - \frac{c_c(x, t) + c_n(x, t)}{S_{tot}}\right) \tag{4}$$

Here, the sorption constants are denoted by k_c and k_a for charged and adsorbed dopants, respectively. The initial conditions for modeling assume that the dopants adsorbed on the surface match the molar fraction first measured by XPS directly after evaporation, and because of the fast incorporation of Mo(tfd-CO$_2$Me)$_3$ into the P3HT film during the evaporation process as observed with IR spectroscopy, a remaining dopant fraction is already distributed evenly within the P3HT film (for details see the Supporting Information). The total concentration of dopants $c(0,t)$ is fitted to the data in Figure 5. For the fitting routine we set S_c fixed since it can be inferred from the data in Figure 4a,c that there is a maximal number of charged dopants. We chose $S_c = 0.05$ for rr-P3HT and $S_c = 0.035$ for rra-P3HT. The sorption constant k_c was set sufficiently high to allow for an immediate charge transfer as observed with IR spectroscopy. From the model fit we then obtain a value of $k_a \approx 0.015$ min^{-1} for both types of P3HT but different values for the total capacity S_{tot}. We get a larger value of S_{tot} for rr-P3HT than for rra-P3HT, meaning that rr-P3HT has a higher capacity or free volume for dopants. The fitted molar fraction of S_{tot} is given by 0.084 for rr-P3HT and 0.058 for rra-P3HT. In order to achieve the best agreement with our experimentally derived data, the diffusion constant D_c has to be high enough to allow for a very fast movement into the bulk, which means that in this case the diffusion process is limited by the dopant uptake. A lower limit of D_c can be estimated and yields $D_c \gtrsim 10^{-15}$ cm^2 s^{-1} for rr-P3HT and $D_c \gtrsim 3 \times 10^{-16}$ cm^2 s^{-1} for rra- P3HT (for details see the Supporting Information).

To understand the differences in Mo(tfd-CO$_2$Me)$_3$ capacity S_{tot} between rr- and rra-P3HT at high concentrations, it is necessary to consider the morphology of such thin films. Electron diffraction measurements (see Figure S12) show that rra-P3HT does not exhibit any signature of crystalline packing. In contrast, the diffraction patterns of rr-P3HT reveal a clear signature of a semicrystalline morphology with crystallites being embedded in an amorphous matrix. These measurements on the materials confirm the results of previous studies.[61] As an amorphous matrix with a slightly lower density rra-P3HT likely has a larger fractional free volume, which would suggest that rra-P3HT would provide a higher free volume than rr-P3HT. However, the observed behavior of the diffusion of Mo(tfd-CO$_2$Me)$_3$ in rra- and rr-P3HT does not follow this trend. There is evidence[62] that the noncrystalline phase in rr-P3HT between the crystalline grains has a lower density than fully amorphous rra-P3HT.

Hence, the regions at grain boundaries in ordered polymers might be important for the diffusion of Mo(tfd-CO$_2$Me)$_3$ in rr-P3HT and as such could offer an explanation for a higher dopant acceptance of rr-P3HT in comparison to rra-P3HT, here observed for dopant layers with $L_d > 14$ nm. The free volume in such regions should also affect the mobility of dopants at low concentrations (in this study, in the beginning of the dopant layer deposition). For example, the mobility model of solvent molecules in polymers (as derived from a statistical treatment) proposes a volatility[44,47] which is given by the relation

$$m_d = A_d e^{-B_d/f} \tag{5}$$

where m_d denotes the mobility, A_d is a shape-dependent proportionality factor, f the fractional free volume, and B_d refers to the void size that dopants require to perform a jump.[46] However, at present there is no proof for this hypothesis which would require the direct identifying and imaging of dopant pathways.

■ CONCLUSION

In summary, we analyzed the penetration of a bulky metal−organic complex acting as p-dopant into a common polymer matrix. The dopant was sequentially evaporated in UHV on rr-P3HT and rra-P3HT films at room temperature. We conclude that the dopant is readily diffusing into the polymer matrix and doping the P3HT film, which is resolved by identifying electron transfer due to characteristic absorption bands in IR spectra and chemical states from XPS binding energies. The diffusion process requires thermal activation energy close to room temperature, which was shown by evaporating dopants on a liquid-nitrogen-cooled rr-P3HT film and subsequent rewarming of the substrate. With IR spectroscopy we can monitor electron transfer during evaporation, which suggests that both rra-P3HT and rr-P3HT quickly incorporate dopants. Differences of the diffusion behavior between rr- and rra-P3HT could be observed from a certain coverage on. Time-dependent XPS measurements allow for determining changes in doping ratios at the surface for varying dopant coverage. We observed a decrease of neutral dopants at the surface for rr-P3HT with time at higher coverage, which is much less apparent for rra-P3HT. The time dependency of sorption and diffusion was numerically modeled, which yields total capacities for dopant uptake in the polymer layers and limits for the diffusion constant at room temperature. Our data show that the sequential doping approach is clearly applicable to the p-doping of P3HT films. On the other hand, in order to prevent an unwanted diffusion of dopants into the full depth of a P3HT film, a fully amorphous interlayer and a controlled filling of voids using a second suitable molecular transport material or redox-inactive molecule could be viable strategies.

■ ASSOCIATED CONTENT

Ⓢ Supporting Information

The Supporting Information is available free of charge on the ACS Publications website at DOI: 10.1021/acs.jpcc.8b02657.

IR and XPS data, TEM data, and additional information on data analysis (PDF)

AUTHOR INFORMATION

Corresponding Authors

*E-mail: sebastian.beck@kip.uni-heidelberg.de (S.B.).

*E-mail: preiser@surface.tu-darmstadt.de (P.R.).

ORCID

Lars Müller: 0000-0001-7321-4702

Robert Lovrincic: 0000-0001-5429-5586

Stephen Barlow: 0000-0001-9059-9974

Seth R. Marder: 0000-0001-6921-2536

Annemarie Pucci: 0000-0002-9038-4110

Eric Mankel: 0000-0001-6566-157X

Sebastian Beck: 0000-0003-2194-6842

Present Address

V.S.: Ruprecht-Karls-Universität Heidelberg, Physikalisch-Chemisches Institut, Im Neuenheimer Feld 253, 69120 Heidelberg, Germany.

Notes

The authors declare no competing financial interest.

ACKNOWLEDGMENTS

We acknowledge the German Federal Ministry of Education and Research (BMBF) for financial support within the InterPhase project (FKZ 13N13656, 13N13657, and 13N13658) and the US National Science Foundation for support through the DMREF program (DMR-1729737). L.M. gratefully acknowledges the scholarship granted by the Carl Zeiss Foundation.

ABBREVIATIONS

Mo(tfd-$CO_2Me)_3$, molybdenum tris(1-(methoxycarbonyl)-2-(trifluoromethyl)ethane-1,2-dithiolene); P3HT, poly(3-hexylthiophene); rr-P3HT, regioregular P3HT; rra-P3HT, regiorandom P3HT.

REFERENCES

(1) Pfeiffer, M.; Fritz, T.; Blochwitz, J.; Nollau, A.; Plönnigs, B.; Beyer, A.; Leo, K. Controlled Doping of Molecular Organic Layers: Physics and Device Prospects. In *Advances in Solid State Physics 39*; Kramer, B., Ed.; Springer: Berlin, 1999; pp 77−90.

(2) Gao, W.; Kahn, A. Effect of Electrical Doping on Molecular Level Alignment at Organic−organic Heterojunctions. *Appl. Phys. Lett.* **2003**, *82* (26), 4815−4817.

(3) Walzer, K.; Maennig, B.; Pfeiffer, M.; Leo, K. Highly Efficient Organic Devices Based on Electrically Doped Transport Layers. *Chem. Rev.* **2007**, *107* (4), 1233−1271.

(4) Pfeiffer, M.; Leo, K.; Zhou, X.; Huang, J. S.; Hofmann, M.; Werner, A.; Blochwitz-Nimoth, J. Doped Organic Semiconductors: Physics and Application in Light Emitting Diodes. *Org. Electron.* **2003**, *4* (2−3), 89−103.

(5) Shen, Y.; Hosseini, A. R.; Wong, M. H.; Malliaras, G. G. How To Make Ohmic Contacts to Organic Semiconductors. *ChemPhysChem* **2004**, *5* (1), 16−25.

(6) Gross, M.; Müller, D. C.; Nothofer, H.-G.; Scherf, U.; Neher, D.; Bräuchle, C.; Meerholz, K. Improving the Performance of Doped π-Conjugated Polymers for Use in Organic Light-Emitting Diodes. *Nature* **2000**, *405* (6787), 661−665.

(7) Ganzorig, C.; Fujihira, M. Improved Drive Voltages of Organic Electroluminescent Devices with an Efficient P-Type Aromatic Diamine Hole-Injection Layer. *Appl. Phys. Lett.* **2000**, *77* (25), 4211−4213.

(8) Zhou, X.; Pfeiffer, M.; Blochwitz, J.; Werner, A.; Nollau, A.; Fritz, T.; Leo, K. Very-Low-Operating-Voltage Organic Light-Emitting Diodes Using a P-Doped Amorphous Hole Injection Layer. *Appl. Phys. Lett.* **2001**, *78* (4), 410−412.

(9) Glaudell, A. M.; Cochran, J. E.; Patel, S. N.; Chabinyc, M. L. Impact of the Doping Method on Conductivity and Thermopower in Semiconducting Polythiophenes. *Adv. Energy Mater.* **2015**, *5* (4), 1401072.

(10) Bubnova, O.; Khan, Z. U.; Malti, A.; Braun, S.; Fahlman, M.; Berggren, M.; Crispin, X. Optimization of the Thermoelectric Figure of Merit in the Conducting Polymer poly(3,4-Ethylenedioxythiophene). *Nat. Mater.* **2011**, *10*, 429.

(11) Hynynen, J.; Kiefer, D.; Muller, C. Influence of Crystallinity on the Thermoelectric Power Factor of P3HT Vapour-Doped with F4TCNQ. *RSC Adv.* **2018**, *8* (3), 1593−1599.

(12) Liu, J.; Qiu, L.; Portale, G.; Koopmans, M.; ten Brink, G.; Hummelen, J. C.; Koster, L. J. A. N-Type Organic Thermoelectrics: Improved Power Factor by Tailoring Host−Dopant Miscibility. *Adv. Mater.* **2017**, *29* (36), 1701641.

(13) D'Andrade, B. W.; Forrest, S. R.; Chwang, A. B. Operational Stability of Electrophosphorescent Devices Containing P and N Doped Transport Layers. *Appl. Phys. Lett.* **2003**, *83* (19), 3858−3860.

(14) Arkhipov, V. I.; Emelianova, E. V.; Bässler, H. Quenching of Excitons in Doped Disordered Organic Semiconductors. *Phys. Rev. B: Condens. Matter Mater. Phys.* **2004**, *70* (20), 205205.

(15) Arkhipov, V. I.; Emelianova, E. V.; Bassler, H. On the Role of Spectral Diffusion of Excitons in Sensitized Photoconduction in Conjugated Polymers. *Chem. Phys. Lett.* **2004**, *383* (1−2), 166−170.

(16) Tyagi, P.; Tuli, S.; Srivastava, R. Study of Fluorescence Quenching due to 2, 3, 5, 6-Tetrafluoro-7, 7′, 8, 8′-Tetracyano Quinodimethane and Its Solid State Diffusion Analysis Using Photoluminescence Spectroscopy. *J. Chem. Phys.* **2015**, *142* (5), 054707.

(17) Ferguson, A. J.; Kopidakis, N.; Shaheen, S. E.; Rumbles, G. Quenching of Excitons by Holes in Poly(3-Hexylthiophene) Films. *J. Phys. Chem. C* **2008**, *112* (26), 9865−9871.

(18) Yamamoto, Y.; Yoshino, K.; Inuishi, Y. Electrical Properties of Phthalocyanine-Halogen Complexes. *J. Phys. Soc. Jpn.* **1979**, *47* (6), 1887−1891.

(19) Kido, J.; Matsumoto, T. Bright Organic Electroluminescent Devices Having a Metal-Doped Electron-Injecting Layer. *Appl. Phys. Lett.* **1998**, *73* (20), 2866−2868.

(20) Parthasarathy, G.; Shen, C.; Kahn, A.; Forrest, S. R. Lithium Doping of Semiconducting Organic Charge Transport Materials. *J. Appl. Phys.* **2001**, *89* (9), 4986−4992.

(21) Tietze, M. L.; Burtone, L.; Riede, M.; Lüssem, B.; Leo, K. Fermi Level Shift and Doping Efficiency in P-Doped Small Molecule Organic Semiconductors: A Photoelectron Spectroscopy and Theoretical Study. *Phys. Rev. B: Condens. Matter Mater. Phys.* **2012**, *86* (3), 35320.

(22) Pingel, P.; Neher, D. Comprehensive Picture of P-Type Doping of P3HT with the Molecular Acceptor F4TCNQ. *Phys. Rev. B: Condens. Matter Mater. Phys.* **2013**, *87* (11), 115209.

(23) Mityashin, A.; Olivier, Y.; Van Regemorter, T.; Rolin, C.; Verlaak, S.; Martinelli, N. G.; Beljonne, D.; Cornil, J.; Genoe, J.; Heremans, P. Unraveling the Mechanism of Molecular Doping in Organic Semiconductors. *Adv. Mater.* **2012**, *24* (12), 1535−1539.

(24) Salzmann, I.; Heimel, G.; Oehzelt, M.; Winkler, S.; Koch, N. Molecular Electrical Doping of Organic Semiconductors: Fundamental Mechanisms and Emerging Dopant Design Rules. *Acc. Chem. Res.* **2016**, *49* (3), 370−378.

(25) Li, J.; Rochester, C. W.; Jacobs, I. E.; Friedrich, S.; Stroeve, P.; Riede, M.; Moulé, A. J. Measurement of Small Molecular Dopant F4TCNQ and C60F36 Diffusion in Organic Bilayer Architectures. *ACS Appl. Mater. Interfaces* **2015**, *7* (51), 28420−28428.

(26) Kang, K.; Watanabe, S.; Broch, K.; Sepe, A.; Brown, A.; Nasrallah, I.; Nikolka, M.; Fei, Z.; Heeney, M.; Matsumoto, D.; et al. 2D Coherent Charge Transport in Highly Ordered Conducting

Polymers Doped by Solid State Diffusion. *Nat. Mater.* **2016**, *15* (8), 896−902.

(27) Gao, W.; Kahn, A. Controlled P-Doping of Zinc Phthalocyanine by Coevaporation with Tetrafluorotetracyanoquinodimethane: A Direct and Inverse Photoemission Study. *Appl. Phys. Lett.* **2001**, *79* (24), 4040−4042.

(28) Duhm, S.; Salzmann, I.; Bröker, B.; Glowatzki, H.; Johnson, R. L.; Koch, N. Interdiffusion of Molecular Acceptors through Organic Layers to Metal Substrates Mimics Doping-Related Energy Level Shifts. *Appl. Phys. Lett.* **2009**, *95* (9), 093305.

(29) Mor, G. K.; Jones, D.; Le, T. P.; Shang, Z.; Weathers, P. J.; Woltermann, M. K. B.; Vakhshouri, K.; Williams, B. P.; Tohran, S. A.; Saito, T. Contact Doping with Sub-Monolayers of Strong Polyelectrolytes for Organic Photovoltaics. *Adv. Energy Mater.* **2014**, *4* (13), 1400439.

(30) Müller, L.; Rhim, S.-Y.; Sivanesan, V.; Wang, D.; Hietzschold, S.; Reiser, P.; Mankel, E.; Beck, S.; Barlow, S.; Marder, S. R. Electric-Field-Controlled Dopant Distribution in Organic Semiconductors. *Adv. Mater.* **2017**, *29*, 1701466.

(31) Gao, W.; Kahn, A. Controlled P Doping of the Hole-Transport Molecular Material N,N′-diphenyl-N,N′-bis(1-Naphthyl)-1,1′-biphenyl-4,4′-diamine with Tetrafluorotetracyanoquinodimethane. *J. Appl. Phys.* **2003**, *94* (1), 359−366.

(32) Qi, Y.; Sajoto, T.; Kröger, M.; Kandabarow, A. M.; Park, W.; Barlow, S.; Kim, E.-G.; Wielunski, L.; Feldman, L. C.; Bartynski, R. A.; et al. A Molybdenum Dithiolene Complex as P-Dopant for Hole-Transport Materials: A Multitechnique Experimental and Theoretical Investigation. *Chem. Mater.* **2010**, *22* (2), 524−531.

(33) Jacobs, I. E.; Aasen, E. W.; Oliveira, J. L.; Fonseca, T. N.; Roehling, J. D.; Li, J.; Zhang, G.; Augustine, M. P.; Mascal, M.; Moule, A. J. Comparison of Solution-Mixed and Sequentially Processed P3HT:F4TCNQ Films: Effect of Doping-Induced Aggregation on Film Morphology. *J. Mater. Chem. C* **2016**, *4* (16), 3454−3466.

(34) Hynynen, J.; Kiefer, D.; Yu, L.; Kroon, R.; Munir, R.; Amassian, A.; Kemerink, M.; Müller, C. Enhanced Electrical Conductivity of Molecularly P-Doped Poly(3-Hexylthiophene) through Understanding the Correlation with Solid-State Order. *Macromolecules* **2017**, *50* (20), 8140−8148.

(35) Fujimoto, R.; Yamashita, Y.; Kumagai, S.; Tsurumi, J.; Hinderhofer, A.; Broch, K.; Schreiber, F.; Watanabe, S.; Takeya, J. Molecular Doping in Organic Semiconductors: Fully Solution-Processed, Vacuum-Free Doping with Metal−organic Complexes in an Orthogonal Solvent. *J. Mater. Chem. C* **2017**, *5* (46), 12023−12030.

(36) Dai, A.; Wan, A.; Magee, C.; Zhang, Y.; Barlow, S.; Marder, S. R.; Kahn, A. Investigation of P-Dopant Diffusion in Polymer Films and Bulk Heterojunctions: Stable Spatially-Confined Doping for All-Solution Processed Solar Cells. *Org. Electron.* **2015**, *23*, 151−157.

(37) Li, J.; Rochester, C. W.; Jacobs, I. E.; Aasen, E. W.; Friedrich, S.; Stroeve, P.; Moulé, A. J. The Effect of Thermal Annealing on Dopant Site Choice in Conjugated Polymers. *Org. Electron.* **2016**, *33*, 23−31.

(38) Berriman, G. A.; Holdsworth, J. L.; Zhou, X.; Belcher, W. J.; Dastoor, P. C. Molecular versus Crystallite PCBM Diffusion in P3HT:PCBM Blends. *AIP Adv.* **2015**, *5* (9), 097220.

(39) Watts, B.; Belcher, W. J.; Thomsen, L.; Ade, H.; Dastoor, P. C. A Quantitative Study of PCBM Diffusion during Annealing of P3HT:PCBM Blend Films. *Macromolecules* **2009**, *42* (21), 8392−8397.

(40) Treat, N. D.; Mates, T. E.; Hawker, C. J.; Kramer, E. J.; Chabinyc, M. L. Temperature Dependence of the Diffusion Coefficient of PCBM in Poly(3-Hexylthiophene). *Macromolecules* **2013**, *46* (3), 1002−1007.

(41) Mills, T.; Kaake, L. G.; Zhu, X.-Y. Polaron and Ion Diffusion in a poly(3-Hexylthiophene) Thin-Film Transistor Gated with Polymer Electrolyte Dielectric. *Appl. Phys. A: Mater. Sci. Process.* **2009**, *95* (1), 291−296.

(42) Kaneto, K.; Agawa, H.; Yoshino, K. Cycle Life, Stability, and Characteristics of Color Switching Cells Utilizing Polythiophene Films. *J. Appl. Phys.* **1987**, *61* (3), 1197−1205.

(43) Li, J.; Koshnick, C.; Diallo, S. O.; Ackling, S.; Huang, D. M.; Jacobs, I. E.; Harrelson, T. F.; Hong, K.; Zhang, G.; Beckett, J.; et al. Quantitative Measurements of the Temperature-Dependent Microscopic and Macroscopic Dynamics of a Molecular Dopant in a Conjugated Polymer. *Macromolecules* **2017**, *50* (14), 5476−5489.

(44) Hedenqvist, M.; Gedde, U. W. Diffusion of Small-Molecule Penetrants in Semicrystalline Polymers. *Prog. Polym. Sci.* **1996**, *21* (2), 299−333.

(45) Frisch, H. L.; Stern, S. A. Diffusion of Small Molecules in Polymers. *Crit. Rev. Solid State Mater. Sci.* **1983**, *11* (2), 123−187.

(46) Fujita, H. Diffusion in Polymer-Diluent Systems. In *Fortschritte Der Hochpolymeren-Forschung*; Springer: Berlin, 1961; pp 1−47.

(47) Cohen, M. H.; Turnbull, D. Molecular Transport in Liquids and Glasses. *J. Chem. Phys.* **1959**, *31* (5), 1164−1169.

(48) Petropoulos, J. H. Quantitative Analysis of Gaseous Diffusion in Glassy Polymers. *J. Polym. Sci. Part A-2 Polym. Phys.* **1970**, *8* (10), 1797−1801.

(49) Koros, W. J.; Paul, D. R. CO_2 Sorption in Poly(ethylene Terephthalate) above and below the Glass Transition. *J. Polym. Sci., Polym. Phys. Ed.* **1978**, *16* (11), 1947−1963.

(50) Paul, D. R.; Koros, W. J. Effect of Partially Immobilizing Sorption on Permeability and the Diffusion Time Lag. *J. Polym. Sci., Polym. Phys. Ed.* **1976**, *14* (4), 675−685.

(51) Dai, A.; Zhou, Y.; Shu, A. L.; Mohapatra, S. K.; Wang, H.; Fuentes-Hernandez, C.; Zhang, Y.; Barlow, S.; Loo, Y.-L.; Marder, S. R.; et al. Enhanced Charge-Carrier Injection and Collection Via Lamination of Doped Polymer Layers P-Doped with a Solution-Processible Molybdenum Complex. *Adv. Funct. Mater.* **2014**, *24* (15), 2197−2204.

(52) Mohapatra, S. K.; Zhang, Y.; Sandhu, B.; Fonari, M. S.; Timofeeva, T. V.; Marder, S. R.; Barlow, S. Synthesis, Characterization, and Crystal Structures of Molybdenum Complexes of Unsymmetrical Electron-Poor Dithiolene Ligands. *Polyhedron* **2016**, *116*, 88−95.

(53) Glaser, T.; Beck, S.; Lunkenheimer, B.; Donhauser, D.; Köhn, A.; Kröger, M.; Pucci, A. Infrared Study of the MoO3 Doping Efficiency in 4,4′-bis(N-Carbazolyl)-1,1′-Biphenyl (CBP). *Org. Electron.* **2013**, *14* (2), 575−583.

(54) Beck, S.; Gerbert, D.; Glaser, T.; Pucci, A. Charge Transfer at Organic/Inorganic Interfaces and the Formation of Space Charge Regions Studied with Infrared Light. *J. Phys. Chem. C* **2015**, *119* (22), 12545−12550.

(55) Kühn, M.; Mankel, E.; Köhn, A.; Mayer, T.; Jaegermann, W. Doping Mechanism of MoO3 in 4,4′-Bis(N-Carbazolyl)-1,1′-Biphenyl: A Photoelectron Spectroscopic Study. *Phys. Status Solidi B* **2016**, *253* (9), 1697−1706.

(56) Müller, L.; Nanova, D.; Glaser, T.; Beck, S.; Pucci, A.; Kast, A. K.; Schröder, R. R.; Mankel, E.; Pingel, P.; Neher, D.; et al. Charge-Transfer−Solvent Interaction Predefines Doping Efficiency in P-Doped P3HT Films. *Chem. Mater.* **2016**, *28* (12), 4432−4439.

(57) Hopkinson, P. E.; Staniec, P. A.; Pearson, A. J.; Dunbar, A. D. F.; Wang, T.; Ryan, A. J.; Jones, R. A. L.; Lidzey, D. G.; Donald, A. M. A Phase Diagram of the P3HT:PCBM Organic Photovoltaic System: Implications for Device Processing and Performance. *Macromolecules* **2011**, *44* (8), 2908−2917.

(58) Tenderholt, A. L.; Szilagyi, R. K.; Holm, R. H.; Hodgson, K. O.; Hedman, B.; Solomon, E. I. Electronic Control of the "Bailar Twist" in Formally D^0-D^2 Molybdenum Tris(dithiolene) Complexes: A Sulfur K-Edge X-Ray Absorption Spectroscopy and Density Functional Theory Study. *Inorg. Chem.* **2008**, *47* (14), 6382−6392.

(59) Mayer, T.; Hein, C.; Mankel, E.; Jaegermann, W.; Müller, M. M.; Kleebe, H.-J. Fermi Level Positioning in Organic Semiconductor Phase Mixed Composites: The Internal Interface Charge Transfer Doping Model. *Org. Electron.* **2012**, *13* (8), 1356−1364.

(60) Amundson, N. R. A Note on the Mathematics of Adsorption in Beds. *J. Phys. Colloid Chem.* **1948**, *52* (7), 1153−1157.

(61) Hugger, S.; Thomann, R.; Heinzel, T.; Thurn-Albrecht, T. Semicrystalline Morphology in Thin Films of poly(3-Hexylthiophene). *Colloid Polym. Sci.* **2004**, *282* (8), 932−938.

(62) Lee, C. S.; Dadmun, M. D. Important Thermodynamic Characteristics of poly(3-Hexyl Thiophene). *Polymer* **2014**, *55* (1), 4−7.

DOI: 10.1021/acs.jpcc.8b02657
J. Phys. Chem. C XXXX, XXX, XXX−XXX